ELSEVIER

Journal of Nuclear Materials 253 (1998) 133–140

journal of nuclear materials

The effect of composition, processing conditions, and irradiation, on lattice defects in spinel ceramics

T.A. Bazilevskaya [a], V.T. Gritsyna [a,*], D.V. Orlinski [b], L.V. Udalova [c], A.V. Voitsenya [a]

[a] *Kharkov State University, Kharkov 310077, Ukraine*
[b] *RSC Kurchatov Institute, Moscow, Russian Federation*
[c] *RNC State Optical Institute, St. Petersburg, Russian Federation*

Abstract

The lattice defects in pure spinel ceramics $MgO \cdot nAl_2O_3$ were investigated as to their dependence on composition, temperature, and time duration of calcination in the course of synthesizing spinel powder. Defects were studied by optical methods measuring absorption and photo-, thermo-, and X-ray-stimulated luminescence. The variation of ceramic composition $0.98 \leq n \leq 1.02$ leads to the formation of different absorption bands: at $n < 1$ absorption bands are present at a wavelength of 480 nm (2.6 eV) with $\Delta E = 0.75$ eV; at $n > 1$ the band is at 620 nm (2.0 eV) with $\Delta E = 0.5$ eV; and at $n = 1$ ceramics are transparent. In luminescence spectra, prominent bands were observed at 253, 370, and 520 nm. Variation of temperature of calcination in the range of 1150–1220°C; duration of calcination of 0.5–2.0 h; and irradiation with X-rays, electrons, and neutrons cause changes in the relative intensities of the absorption and luminescence bands, which makes identifying the nature of lattice defects in spinel ceramics possible. © 1998 Elsevier Science B.V.

1. Introduction

Many insulating materials are required for instrumentation in fusion reactors and other technological applications, which may be subjected to high doses of radiation [1]. In these cases, the materials must be able to withstand different ionizing and displacing irradiation at elevated temperatures. Today, most insulators recommended for these applications are metal oxides such as MgO, Al_2O_3, and $MgAl_2O_4$ in single crystalline or ceramic form [2]. The high radiation resistance of spinel upon exposure to high fluences of neutrons (radiation resistance relates to minimal changes in microstructure, elastic constants, microhardness, and swelling) is well known [3–6]. For technological purposes, there is a need for parts with large volumes and complicated shapes; this leads to the impossibility of using single crystals. These problems could be solved by using ceramic technology. Properties of spinel ceramics fabricated by conventional hot-pressing methods are complex functions of processing temperature (thermodynamics) and sintering time (kinetics). Both factors influence the type and concentration of defects and the cation distribution in spinel ceramics. By varying the composition and processing (calcination and sintering) parameters, spinel ceramics of optical quality were fabricated [7]. In this paper, we report on the optical properties of fabricated and irradiated spinel ceramics.

2. Experimental procedure

2.1. Sample preparation

Magnesium aluminate spinel was synthesized by solid state reactions between two substances: ammonium aluminum sulfate, $NH_2Al(SO_4)$, and magnesium sulfate, $MgSO_4 \cdot 7H_20$. Starting substances were melted in platinum crucibles and placed in a calcination furnace using different temperatures (1150–1220°C) for different times

* Corresponding author. Tel.: +380-572 35 2711; fax: +380-572 35 3977; e-mail: gritsyna@pem.kharkov.ua.

PII S0022-3115(97)00340-1

(0.5–2.0 h). Intermediate spinel compositions $MgO \cdot nAl_2O_3$ with $0.98 \leq n \leq 1.02$ were synthesized by mixing different ratios of starting substances. The calcination product was combined with acetone and ground in an agate mortar. Then the powder was sifted through wire-gauze of 6400 mesh/cm^2. The grain size of the final spinel powder was about 0.5–0.7 μm. This fine precursor spinel powder was pressed and sintered at a temperature of 1380°C at a pressure of 1.5 T/cm^2 for 60 min. Disks of 10 cm in diameter and 8 mm in thickness were cut into slices for experimental investigations. The dimensions of fabricated plates for optical measurements were 20×20 mm and 0.5–2.0 mm in thickness. Both sides of the plates were polished to an optical finish.

2.2. Optical measurements

The spinel ceramic samples were characterized by measuring optical absorption in the wavelength range 190–830 nm (6.5–1.5 eV), using a two-beam spectrophotometer. Photoluminescence spectra were also obtained in the wavelength range 200–800 nm (6.2–1.5 eV), by exposure to light from a mercury lamp through a light filter with a maximum wavelength of 360 nm (3.4 eV). X-ray-stimulated luminescence was measured in the wavelength range 200–800 nm (6.2–1.5 eV), by excitation with X-rays using a Cu or Fe X-ray tube operated at 40 kV and 10 mA. Finally, the thermo-stimulated luminescence of spinel samples irradiated with X-rays was investigated by measuring glow curves in the spectral range 190–230 nm (6.5–5.4 eV) and in the temperature range 200–700 K using a heating rate of 0.2 K/s.

2.3. Irradiation of samples

Spinel samples were irradiated with X-rays using an Fe anode X-ray tube operating at 40 kV and 2.5 mA; this corresponds to a dose rate of 10^3 R/min. For electron irradiations a 10-MeV linear electron accelerator with a pulsed beam of $\sim$3-μs duration and frequency of 50 pulses/s was used. Irradiation doses were measured near the sample position. The average flux of electrons was $3–5 \times 10^{12}$ e$^-$/cm^2 s. Combined gamma and neutron irradiations were performed in a nuclear reactor at the Kurchatov Institute. The neutron flux with $E_n < 0.1$ MeV was 2.5×10^{12} n/cm^2 s; the gamma dose rate was 85 Gy/s. The temperature of specimens during irradiations was maintained at ≤ 30°C.

3. Experiment results

It should be noted that for fixed processing conditions (even using one experimental apparatus), one can obtain ceramics with different properties. This implies that there are uncontrolled variations in processing conditions; consequently, the optical properties of ceramics will be different because of the high sensitivity to the preparation methods used. So, results given in this paper are verified statistically by examining numerous process sequences on spinel samples. It has been shown elsewhere [8] that doping spinel with Mn produces ceramics whose properties are less sensitive to composition, calcination, and sintering parameters. We will not include the influence of hot-pressing parameters in our discussion here.

3.1. Variation of spinel composition

To produce optically-transparent spinel ceramics, we varied the composition of spinel powder by changing the ratios of the constituents (MgO, Al_2O_3). This leads to changes in the value of n in spinel ceramics, $MgO \cdot nAl_2O_3$. We will discuss effects of variations in n in the region $0.98 \leq n \leq 1.02$, as we obtained optically transparent ceramics of different colors in this range of n. (It should be noted that for values of $n > 1.05$, we obtained homogeneous spinel ceramics, but none are transparent, while at $n < 0.97$, the ceramics we produced were heterogeneous with many inclusions.)

Typical absorption spectra of spinel ceramics with different n are shown in Fig. 1. For $n > 1.01$, the absorption spectra contain a rather prominent absorption band at 2.0 eV (620 nm). Absorption increases rapidly with increasing photon energy. Some samples exhibited another band at 2.8 eV (440 nm). In absorption spectra in ceramics with

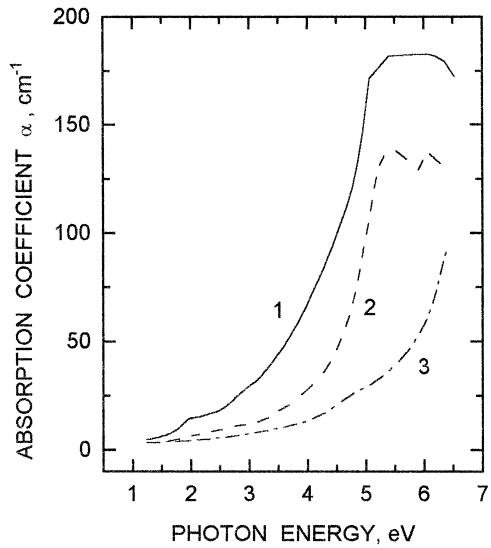

Fig. 1. Absorption spectra of spinel ceramics $MgO \cdot nAl_2O_3$ of different composition $n = 1.02$ (1), $n = 0.98$ (2) and $n = 1.00$ (3).

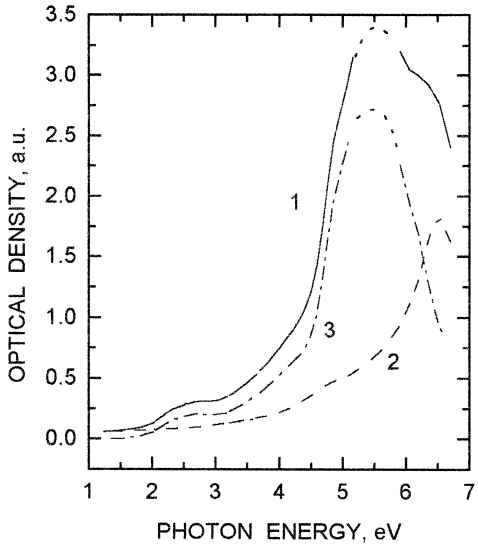

Fig. 2. Absorption spectra of spinel ceramics $MgO \cdot nAl_2O_3$ with $n = 0.98$ (1) and $n = 1.00$ (2). Spectrum (3) is the difference between spectra (1) and (2).

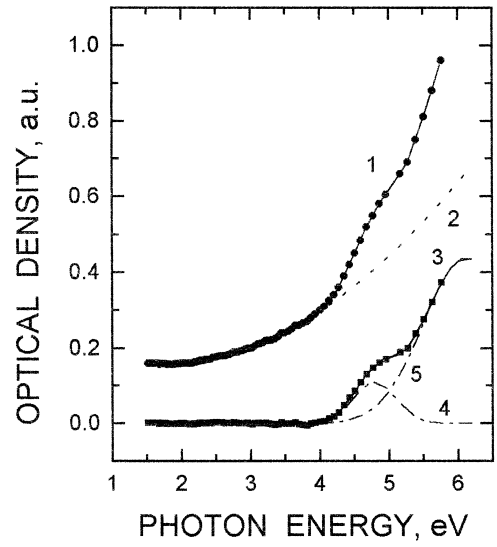

Fig. 3. Absorption spectra of spinel ceramics with composition $MgO \cdot 1.00Al_2O_3$ (1) and correction for background $D \sim E^2$ (2). Spectrum (3) is obtained by subtracting the background fit (2) from spectrum (1). (4) and (5) are Gaussian functions used to fit spectrum (3).

$n < 1$, an absorption band with a maximum at 2.6 eV (480 nm) appeared, along with a prominent absorption band at 5.4 eV (230 nm). Absorption spectra for spinel ceramics with $n = 1$ exhibit only weak absorption, though an absorption band at 4.8 eV (260 nm) could be distinguished. At this point, we conclude that the prominent absorption bands in spinel ceramics with $n < 1$ and $n > 1$ may be attributed to deviations of composition from the equimolar stoichiometry. So, absorption band features in absorption spectra from non-stoichiometric ceramics can be attributed to point defects associated with non-stoichiometry. The low-energy absorption bands in non-stoichiometric spinel samples are more clearly distinguished by observing 'difference' spectra in which the absorption spectrum for $n = 1$ is subtracted from spectra for non-stoichiometric samples ($n \neq 1$) (Fig. 2). Using Gaussian peak-shape profiles for absorption bands, we determined that for non-stoichiometric spinel, the full-width at half-maximum (FWHM) of the 2.0 eV (620 nm) band is 0.5 eV, while the FWHM of the 2.6 eV (480 nm) band is 0.75 eV.

In Fig. 3, an absorption spectrum obtained from a spinel ceramic with $n = 1$ was fit in the low-energy regime, with an absorption function that varied as the second power of the photon energy. Subtracting this function from the original spectrum, an absorption band centered at 4.8 eV (260 nm) with $\Delta E = 0.7$ eV was revealed.

In X-ray-stimulated luminescence spectra (Fig. 4), we found three prominent bands related to transitions localized on lattice defects and one at 2.4 eV (520 nm) related to impurity Mn [9]. The former bands are centered at wavelengths 4.9 eV (253 nm), 3.4 eV (360 nm), and 3.0 eV (410 nm). The clearly resolved band at 253 nm is very intense for spinel ceramics with $n = 1.02$. The intensities of the other bands also depend on the composition of the spinel.

The spectra from photo-stimulated luminescence measurements (not shown), using photons with energy 3.4 eV (360 nm), contain a band at 2.4 eV (520 nm) and a wide band centered at 2.5 eV (490 nm) with $\Delta E = 0.9$ eV.

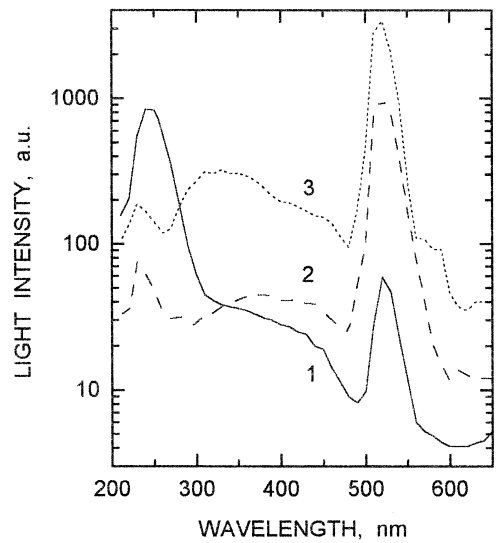

Fig. 4. Spectra of X-ray-stimulated luminescence from spinel ceramics $MgO \cdot nAl_2O_3$ of different compositions: $n = 1.02$ (1), $n = 0.98$ (2) and $n = 1.00$ (3).

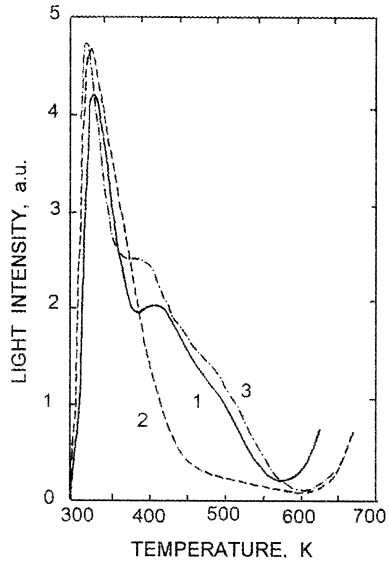

Fig. 5. Glow curves from X-ray-irradiated spinel ceramics $MgO \cdot nAl_2O_3$ of different composition: $n = 1.02$ (1), $n = 0.98$ (2), and $n = 1.00$ (3).

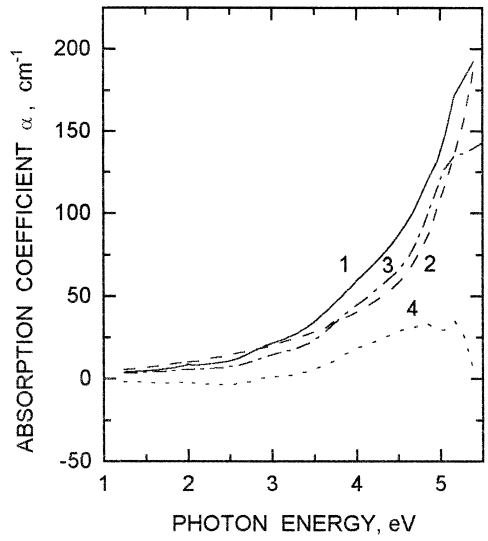

Fig. 6. Absorption spectra from spinel ceramics with composition $MgO \cdot 1.00Al_2O_3$, sintered from powder which was calcined for 2 h at different temperatures: 1150°C (1), 1200°C (2), and 1220°C (3). Spectrum (4) is the difference between spectra (1) and (2).

The glow curves of spinel ceramics irradiated with X-rays are shown in Fig. 5. The main glow peak at 335 K was observed in all samples with slightly different intensities. The FWHM of these glow peaks was 60, 75, and 50 K for $n > 1$, $n < 1$, and $n = 1$, respectively. But the intensities of peaks at higher temperatures are very sensitive to the compositions of the spinel ceramics. For $n < 1$, these higher temperature peaks are nearly absent.

3.2. Variation of calcination parameters

Two parameters were changed during the calcination process of the ceramics powders: the temperature of calcination at a fixed sintering time, and the calcination time at fixed temperature. Fig. 6 shows absorption spectra of spinel ceramics with $n = 1$ prepared at different calcination temperatures. Variation in temperature for 2 h of calcination leads to perceptible changes in absorption bands at 4.0 eV (310 nm) and 4.8 eV (260 nm). X-ray-stimulated luminescence spectra are very sensitive to the temperature of calcination, indicating that changes in point defect chemistry occur over a rather narrow temperature range for calcination. At temperatures of 1150°C and 1220°C, the intensity of the UV band is lower than that of visible bands (Fig. 7). At the temperature of 1200°C, the situation is reversed. Moreover, using a temperature of 1200°C for calcination and a shorter calcination time (1 h) leads to tremendous growth of the 253-nm luminescent band.

Glow curves of spinel ceramics sintered at different temperatures and irradiated with X-rays are shown in Fig. 8. Low temperature calcination yields a very complicated glow curve with maxima at 370, 420, and 550 K. At medium calcination temperatures, the glow curve has two maxima very similar to spinel single crystal curves [10]. High temperature calcination leads to a reconstruction of glow curves with a maximum appearing at 340 K. Time dependencies of absorption spectra from spinel ceramics calcined at a fixed temperature of 1200°C are shown in Fig. 9. We can see that an optimal time for calcination (1.5 h) yields lower absorption in the visible region (absorption is shifted into the UV).

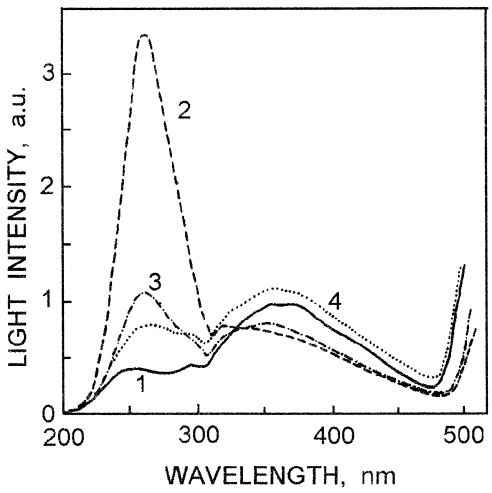

Fig. 7. X-ray-stimulated luminescence spectra from spinel ceramics with composition $MgO \cdot 1.00Al_2O_3$, sintered from powder that was calcined under the following conditions: 1150°C – 2 h (1), 1200°C – 1 h (2), and 1200°C – 2 h (3), and 1220°C – 2 h.

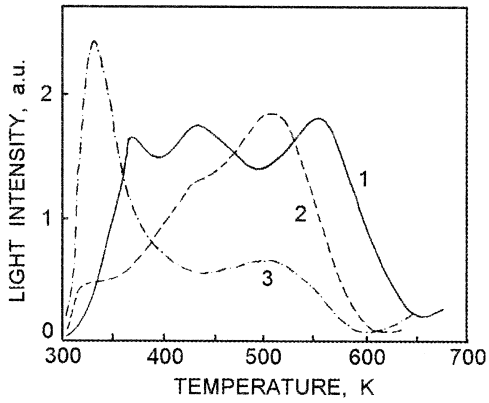

Fig. 8. Glow curves for spinel ceramics with composition $MgO \cdot 1.00Al_2O_3$, sintered from powder that was calcined for 2 h at different temperatures: 1150°C (1), 1200°C (2), and 1220°C (3).

3.3. Influence of irradiation

X-ray irradiation of spinel ceramics of different compositions causes increased absorption in a broad wavelength band centered at 3.1 eV (400 nm). We identify this band with hole-centers at cation vacancies in spinel. Irradiation with 10-MeV electrons to different doses yields an absorption band at 3.1 eV (400 nm) along with additional absorption bands at 5.4 eV (230 nm), 4.4 eV (280 nm), and 3.8 eV (330 nm).

Radiation-induced absorption ($\Delta\alpha$) spectra for spinel ceramics with $n < 1$ subjected to 10 MeV electron irradiation to different doses are shown in Fig. 10. The $\Delta\alpha$ for bands at 3.8 eV (330 nm) and 5.4 eV (230 nm) vary with electron dose.

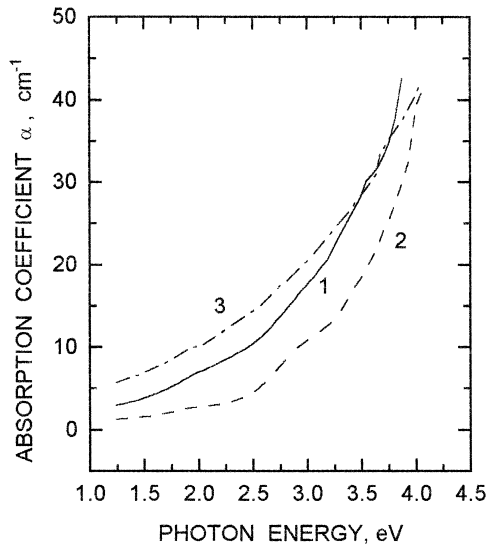

Fig. 9. Absorption spectra from spinel ceramics with composition $MgO \cdot 1.00Al_2O_3$, sintered from powder that was calcined at 1200°C for: 1 h (1), 1.5 h (2), and 2 h (3).

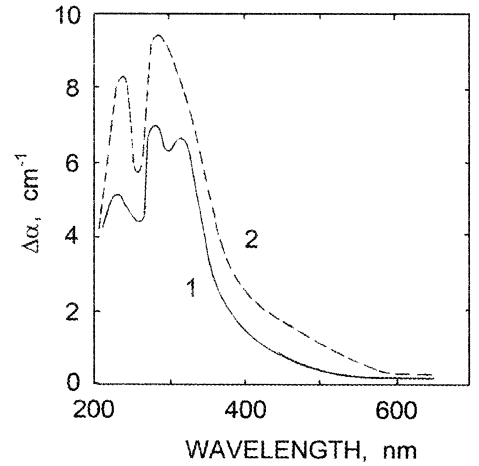

Fig. 10. Radiation-induced absorption spectra for spinel ceramics with composition $MgO \cdot 0.99Al_2O_3$, following irradiation with 10-MeV electrons to doses of 1.35 MGy (1) and 8.0 MGy (2).

Fig. 11 shows X-ray-stimulated luminescence spectra from spinel ceramics with $n < 1$ irradiated with 10-MeV electrons. In the UV region, three bands are apparent that peak at 4.9 eV (253 nm), 4.4 eV (280 nm), and 3.4 eV (360 nm). The intensities of these bands depend on the radiation dose, while the two bands visible at 2.4 eV (520 nm) and 1.8 eV (680 nm) do not vary with increasing electron dose.

Neutron- and gamma-irradiation-induced absorption spectra of spinel ceramics with $n < 1$ are shown in Fig. 12.

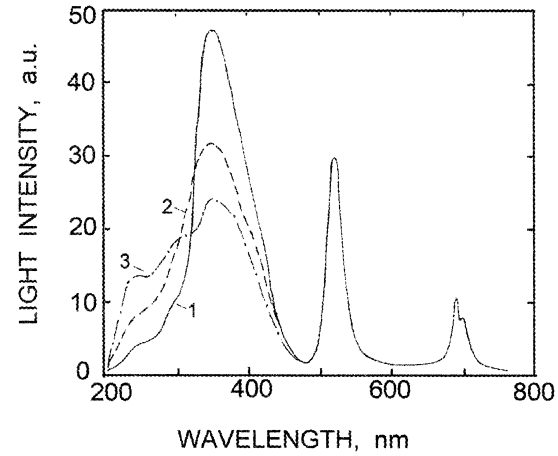

Fig. 11. X-ray-stimulated luminescence spectra for spinel ceramics with composition $MgO \cdot 0.99Al_2O_3$, unirradiated (1) and irradiated with 10-MeV electrons to doses of 1.35 MGy (2) and 8.0 MGy (3).

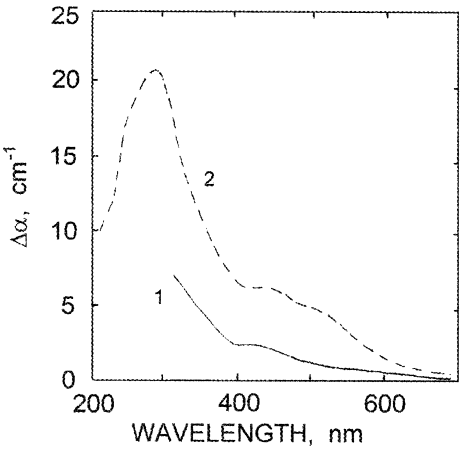

Fig. 12. Radiation-induced absorption spectra for neutron-irradiated spinel ceramics with composition $MgO \cdot 0.98Al_2O_3$, irradiated to fluences of 6×10^{14} (1) and 6×10^{15} neutrons/cm^2 (2).

At low neutron fluence, an absorption band at 2.8 eV (440 nm) appeared. After irradiation to 6×10^{15} neutrons/cm^2, additional absorption bands appeared at 2.5 eV (500 nm) and 4.4 eV (280 nm).

4. Discussion

4.1. Effects of composition and calcination parameters on properties of spinel ceramics

First we discuss the influence of composition on the optical properties of spinel ceramics. We know [11] that magnesium aluminate spinel is a solid solution between MgO and Al_2O_3, such that compounds $MgO \cdot nAl_2O_3$ exist with the spinel structure over a compositional range from $1 \le n \le 7$. The conventional, cubic unit cell of stoichiometric spinel contains 8 $MgAl_2O_4$ molecules and has the cubic space group Fd3m. The oxygen ions are arranged in an almost cubic close-packed structure. Such an arrangement of oxygen results in 64 tetrahedral and 32 octahedral sites for cations per unit cell, of which 8 tetrahedral sites are occupied by Mg^{2+} ions, and 16 octahedral sites are occupied by Al^{3+} ions. This so-called 'normal spinel structure' is present only in natural spinel crystals. For synthetic spinel crystals grown in a laboratory, a fraction x of Al^{3+} ions occupy tetrahedral sites, and an equal fraction of Mg^{2+} ions occupy octahedral sites. Consequently, spinel structures are characterized by the additional parameter x, the degree of disorder, and the chemical formula is rewritten $(Mg_{1-x}Al_x)[Mg_xAl_{2-x}]O_4$. In the case of non-stoichiometric spinel crystals with $n > 1$, the additional absorption appearing in the UV region may be related to defects of non-stoichiometric nature. In $MgO \cdot nAl_2O_3$ with $n > 1$, excess Al^{3+} ions replace Mg^{2+} ions, and in order to maintain charge neutrality, cation vacancies are formed [12,13]. As indicated in Section 2.1, the starting material we used for hot-pressing procedures consisted of a fine powder with grain sizes ranging from 0.5–0.7 μm. For $n > 1$ spinel ceramics, additional cation vacancies are formed, and we may expect a non-uniform distribution of these vacancies throughout the grains of the ceramics. Also, these defects may decorate surfaces or grain boundaries. During hot-pressing, these interface regions play an important role in obtaining spinel ceramics near theoretical density. An excess of cation vacancies near interfaces might lead to the creation of vacancy defect complexes. But due to the low calcination and hot-pressing temperatures used here, only a small fraction of point defects can agglomerate into defect complexes. This conclusion follows from the fact that estimates of diffusion lengths, $(Dt)^{1/2}$, for diffusivity (D) of defects over reasonable times (t), are on the order of a lattice parameter or less. Nevertheless, we believe that cation vacancy complexes formed during processing are responsible for the absorption band observed at 620 nm in $n > 1$ spinels.

For $n < 1$ spinel ceramics, anion vacancies and their complexes are probably formed. We tentatively ascribe the absorption band at wavelength 480 nm to optical transitions centered on anion vacancy complexes. Upon X-ray irradiation, some increase in the intensity of this band was observed. The large width of this band suggests that several types of anion vacancy complexes are present with a variety of energies of trapped electrons in their centers. There is some evidence for this identification, because for spinel samples with $n < 1$, we observe an additional prominent absorption band at 230 nm, which can be attributed to transitions at isolated point defect centers in spinel single crystals [14].

In practice, it is impossible to fabricate spinel ceramics with $n = 1$; so, some samples with n values nominally equal to 1 could be attributed to the beginning of the formation of non-stoichiometric spinel with $n < 1$, and others with $n > 1$. In Fig. 3, the absorption spectra of spinel ceramics with a nominal n value of 1, but with measured $n = 0.998$, exhibit only one minor band at 260 nm, which is related to F^+-centers in spinel.

To determine the relationships between different defects and their radiative processes, we investigated X-ray-stimulated luminescence spectra (Fig. 4) from spinel ceramics with different compositions. We found that luminescence spectra have several bands that peak at wavelengths of 253 nm, 360 nm, and 520 nm. The last band is related to a transition in impurity of Mn^{2+} ions and will not be discussed in this paper. The relative intensity of this band is also a function of n. We can see that the highest intensity of this band occurs in the case of stoichiometric spinel ceramics (interestingly, the intensity varies even though the concentration of Mn is nominally the same in all samples). In a previous investigation, the luminescence band at 360 nm was identified with transitions occurring at F-type centers. The highest intensity of this band was

observed for spinel with $n < 1$; this is in agreement with the supposition made above. The band centered at wavelength 253 nm is most intense for spinel ceramics with $n > 1$. Let us consider the possible nature of this band and its intensity-dependence on the composition of spinel ceramics. As discussed at the beginning of this section, synthetic spinel crystals (fabricated in the laboratory) have some degree of inversion (usually $0.1 < x < 0.3$). Upon inversion, Mg^{2+} ions situated on octahedral lattice sites form centers with excess negative charge. During irradiation a free hole could be trapped at this defect, thus neutralizing it, as denoted by the following reaction:

$$\left[\mathrm{Mg}_{\mathrm{Al}}^{2+}\right]^{-} + \mathrm{h} \rightarrow \left[\mathrm{Mg}_{\mathrm{Al}}^{2+}\right]^{0}. \quad (1)$$

Also accompanying the inversion process, Al^{3+}-ions will be located at tetrahedral sites, forming centers with excess positive charge. Upon irradiation, these centers will trap electrons to form charge-neutral centers, denoted by

$$\left(\mathrm{Al}_{\mathrm{Mg}}^{3+}\right)^{+} + \mathrm{e}^{-} \rightarrow \left(\mathrm{Al}_{\mathrm{Mg}}^{3+}\right)^{0}. \quad (2)$$

Because of the low energy of the electron affinity to Al^{3+} at room temperature, captured electrons will likely leave this trap and recombine with a nearby trapped hole on an octahedral site.

This reaction is accompanied by a release of energy in the form of quantum light with a wavelength of 253 nm:

$$\left[\mathrm{Mg}_{\mathrm{Al}}^{2+}\right]^{0} + \mathrm{e}^{-} \rightarrow \left[\mathrm{Mg}_{\mathrm{Al}}^{2+}\right]^{-} + h\nu\ (253\ \mathrm{nm}). \quad (3)$$

We can suppose that the most favorable conditions to create nearby antisite defects (Mg_{Al} and Al_{Mg}) are in spinel ceramics with $n > 1$. This suggestion is verified by the thermally stimulated luminescence of X-ray-irradiated spinel ceramics with different n. Investigations of the spectral composition of glow curves indicate that glow peaks with a maximum at 335 K mostly consist of UV-emission with a wavelength of 253 nm [9]. Also, heating the sample under X-ray irradiation leads to an increase of intensity of this band in X-ray-stimulated luminescence. This implies that the recombination processes for charge carriers trapped on antisite defects are also responsible for glow peaks with a maximum at 335 K. The difference in processes of X-ray-stimulated and thermally stimulated luminescence is in the distance between antisite defect pairs. For large pair separations (third, fourth, etc., coordination sphere) between captured electrons and holes, some activation energy is needed to transport electrons to hole centers. The spatial distribution of captured charge carriers will influence the width of glow peak. From experimental data, the most homogeneous distribution (i.e., captured carriers in closest proximity) is for stoichiometric spinel ceramics. For spinel with $n < 1$, anion vacancies will have some influence on spatial distribution of antisite defects and on the depth of electron traps.

The variation of sintering parameters, for fixed composition spinel ceramics, influences kinetics of defects formation and their spatial distribution. Variation in the temperature of calcination leads to a change in absorption in the UV-region (Fig. 6). The difference in absorption spectra of spinel calcined at 1150, 1200, and 1220°C indicates a trade-off between absorption in the UV-region (isolated anion defects) and visible region (complexes of defects). In X-ray-stimulated luminescence experiments (Fig. 7), at low temperatures of calcination, we observed high intensity for luminescence related to F-centers (wavelength 360 nm). But at 1200°C, optimal conditions are present for the creation of spinel structure with nearby antisite defect pairs and a low concentration of isolated F-centers.

4.2. Effects of irradiation on properties of optical spinel ceramics

Irradiation of spinel ceramics with fast electrons up to 8.0 MGy causes additional absorption bands mostly in the UV-region. Because of the large value (α) of starting ceramics, the different spectra of irradiated and non-irradiated samples have a rather large scattering. In radiation-induced absorption spectra we can find bands with maxima at 230, 280, and 330 nm, and a wide band near 400 nm. The last one can be identified with absorption by V-type centers in irradiated spinel; the bands at 230 and 280 nm are related to F-type centers in spinel [14]. At the higher irradiation dose, there are two absorption bands at 330 nm and 440 nm that may be related to centers at antisite defects [15]. To obtain an irradiation dose of 8.0 MGy, the samples were irradiated to electron fluence of 10^{16} e^{-}/cm^{2} with an energy of 10 MeV; this produces about 6×10^{16} defects/cm^{3}. Similar behavior of absorption bands centered at 230 and 280 nm indicated the same origin of defects: anion vacancies capture two (F-center) or one (F^{+}-center) electron. From the measured $\Delta\alpha$ of these bands, we can estimate the increase in concentration of F-type centers upon electron irradiation. We find an F-center concentration of 3×10^{15} cm^{-3} at 8.0 MGy electron dose. This implies that only 1/20th of lattice defects produced by irradiation survive as F-centers. Also, the increase in absorption bands at 330 and 440 nm upon electron irradiation may indicate the occurrence of charge carrier trapping at radiation-induced antisite defect centers (such as the reactions described in Eqs. (1) and (2)). X-ray-stimulated luminescence shows the decrease of luminescence band intensity at 360 nm, related to F-type centers and enhancement of luminescence band at 253 nm. As discussed before, the last band is connected with recombination luminescence at antisite defects; so, luminescent data are consistent with absorption data. The de-

crease of luminescence intensity of F-type centers, despite an increase in their concentration, could be explained by concentration quenching, or a transfer of excitation energy to non-radiative channels.

For gamma-neutron irradiated samples, absorption spectra revealed absorption bands at 440, 330, and 280 nm, but the band with maximum at wavelength 230 nm (observed in electron-irradiated samples) is lacking. Neutron irradiation to a fluence of 6×10^{15} n/cm^2 (energy $>$ 0.1 MeV) creates more than 10^{16} F^+ centers/cm^3. Note that radiation-induced cation disorder leads to formation of absorption bands at the irradiation-induced antisite defects. The thermodynamically induced cation disorder does not show any absorption bands.

5. Conclusions

Investigating the properties of spinel ceramics fabricated by the hot-pressing method using a variety of compositions, processing temperatures, and calcination times, allowed us to determine parameters for obtaining homogeneous optical ceramics. Using optical measurements we investigated properties of point defects associated with both anion and cation spinel sublattices, point defect complexes, and antisite defects. For a variety of spinel samples, we investigated the influence of X-ray, electron, and neutron irradiations on the following optical properties: absorption-, X-ray-, photo- and thermo-stimulated luminescence. Using low doses of radiation and methods sensitive to low concentration of defects, we obtained knowledge about the initial stages of defect creation in spinel ceramics for different irradiation conditions.

Acknowledgements

The authors wish to thank Mrs N.A. Bessonova for sample preparation and Mr I.V. Afanasiev for substantial help in preparing this manuscript.

References

[1] F.W. Clinard Jr., G.F. Hurley, R.W. Klaffky, Res. Mech. 8 (1983) 207.
[2] R. Heidinger, J. Nucl. Mater. 64 (1991) 179.
[3] S.J. Zinkle, E.R. Hodgson, J. Nucl. Mater. 58 (1992) 191.
[4] C. Kinoshita, S.J. Zinkle, J. Nucl. Mater. 100 (1996) 233.
[5] S.J. Zinkle, J. Nucl. Mater. 113 (1995) 219.
[6] F.A. Garner, G.W. Hollenberg, F.D. Hobbs, J.L. Ryan, Z. Li, C.A. Black, R.C. Bradt, J. Nucl. Mater. 1087 (1994) 212.
[7] V.M. Maltsev, L.V. Udalova, N.A. Bessonova, I.A. Naumova, Sov. J. Opt. Technol. 1 (1993) 55.
[8] T.A. Bazilevskaya, G.I. Belikh, V.T. Gritsyna, N.A. Bessonova, M.G. Karpenko, M.V. Maltsev, L.V. Udalova, Invention N1715774, USSR.
[9] V.T. Gritsyna, V.A. Kobyakov, N.A. Mironova, V.N. Skvortsova, N.A. Damburg, Izv. AN Latv. SSR. Phys. Techn. Sci. 5 (1983) 26.
[10] V.T. Gritsyna, T.I. Voitsenya, T.I. Korneeva, V.B. Kolner, A.M. Pshisukha, Sov. Phys. JETP 50 (1980) 2220.
[11] S. Hafner, F. Laves, Z. Kristallogr. 115 (1961) 321.
[12] R. Dupree, M.H. Lewis, M.E. Smith, Philos. Mag. A 53 (1986) L17.
[13] A. Ibarra, V. Vila, M. Jimenez de Castro, Philos. Mag. Lett. 64 (1991) 45.
[14] L.S. Cain, G.J. Pogatshnik, Y. Chen, Phys. Rev. B 37 (1988) 2645.
[15] G.S. White, R.V. Jones, J.H. Crawford Jr., J. Appl. Phys. 53 (1982) 265.